9008 *Macromolecules* **2009**, *42*, 9008–9017
DOI: 10.1021/ma901432v

Macromolecules
ARTICLE

Crystallization of Molecular Brushes with Block Copolymer Side Chains

Sherryl Y. Yu-Su and Sergei S. Sheiko*

Department of Chemistry, Caudill and Kenan Laboratories, The University of North Carolina at Chapel Hill, Chapel Hill, North Carolina 27599

Hyung-il Lee,[†] Wojciech Jakubowski,[‡] Alper Nese, and Krzysztof Matyjaszewski

Center for Macromolecular Engineering, Department of Chemistry, Carnegie Mellon University, 4400 Fifth Avenue, Pittsburgh, Pennsylvania 15213

Denis Anokhin and Dimitri A. Ivanov*

Institut de Sciences des Matériaux de Mulhouse CNRS LRC 7228, 15 rue Jean Starcky, B.P. 2488, 68057 Mulhouse Cedex, France. [†]Current address: Department of Chemistry, University of Ulsan, Ulsan 680-749, Republic of Korea. [‡]Current address: ATRP Solutions, 166 N Dithridge, Suite G4, Pittsburgh, PA 15213

Received July 2, 2009; Revised Manuscript Received October 22, 2009

ABSTRACT: A series of three cylindrical molecular brushes with poly(ε-caprolactone)-*b*-poly(*n*-butyl acrylate) side chains were investigated with regard to the effect of the intramolecular confinement on the crystallization behavior of the PCL core block. While the length of the PCL block was maintained (n_{PCL} = 50), the degree of polymerization of the PBA corona block, prepared by atom transfer radical polymerization, was varied from n_{PBA} = 0 (PCL brush) to n_{PBA} = 52 and 163. The crystallization behavior of the studied polymers was shown to be different in thin films and bulk samples. In thin films, the brushlike macromolecules were fully extended and remained segregated due to the steric repulsion of the adsorbed PBA corona. Under the constraint of the backbone extension, crystallization of the PCL core led to formation of a characteristic spinelike morphology. In bulk samples, the core−shell confinement did not prohibit breakout crystallization, leading to the formation of a spherulitic morphology similar to linear and brushlike PCL. However, the crystallization process of the PCL-*b*-PBA brushes was significantly slower as compared to the linear and brushlike counterparts as it evolved through a transition from the molecularly segregated core−shell morphology to a lamellar organization of multiple molecules. Drawing of fibers containing nascent crystallites resulted in the final morphology composed of crystalline lamellae parallel to the fiber axis with the PCL blocks oriented perpendicular to the axis. The lamellae thickness was shown to decrease with the length of the amorphous PBA block.

Introduction

Because of the large size and chainlike nature of polymer molecules, morphology of semicrystalline polymers is, at any given instance, kinetically controlled. Crystallization of the slow-moving flexible macromolecules results in metastable morphologies with a degree of crystallization which generally never attains 100%.[1,2] It is also challenging to control the shape of crystallites and the alignment of polymer chains that largely determine the physical properties of industrial plastics. One of the general strategies to manage the molecular packing is to introduce spatial constraints. For example, crystallization of polymer chains in mesoscopic pores[3−6] may lead to chain orientation, provided that the pores are much smaller than the radius of gyration of the chain. However, this approach requires preparation of a composite material composed of a polymer and a porous matrix. An alternative way to constrain polymer chains is to exploit the microphase separation of block copolymers,[7,8] which inherently provides nanometer-sized domains of crystalline blocks imbedded into a matrix of the amorphous block.[9,10] Yet, in many cases, the block copolymer domains are unable to confine the crystallization process, leading to the so-called "breakout crystallization".[11]

Here, we investigate the crystallization behavior of molecular brushes with diblock copolymer side chains that result in a core−shell molecular structure possessing a crystallizable core and an amorphous corona.[12] Similar to diblock copolymers, this type of molecular brush is subject to the interplay of two microphase separation processes: (i) demixing of the chemically different blocks and (ii) crystallization of the core block. However, there are several distinctive features. First, the brush molecules intrinsically prefer a cylindrical shape stabilized by the steric repulsion between densely grafted side chains.[13−17] Second, the brushlike architecture imposes an additional constraint to the crystalline block due to its covalent linkage to the backbone. Third, the steric repulsion causes disentanglement of polymer chains and thus facilitates molecular alignment. One expects that the additional topological constraints, along with the enhanced molecular segregation, will provide new tools for controlling both the crystallization process and the resulting morphology.

In this paper, the crystallization behavior of densely grafted brushes with diblock copolymer side chains composed of a

*Corresponding authors. E-mail: sergei@email.unc.edu (S.S.S.); dimitri.ivanov@uha.fr (D.A.I.).

 Published on Web 11/03/2009

Scheme 1. Synthesis of Molecular Brushes with PCL (IA) and Block Copolymer PCL-*b*-PBA (IIA) Side Chains[12] [a]

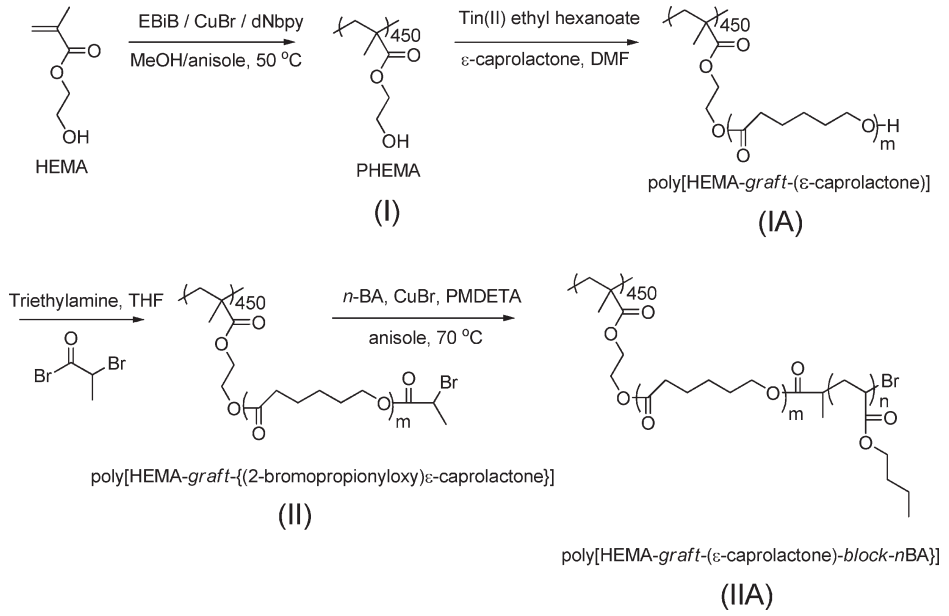

[a] The PCL brushes have been used as precursor for the synthesis of the block copolymer brushes.

semicrystalline poly(ε-caprolactone) block (PCL) and an amorphous poly(*n*-butyl acrylate) (PBA) block is presented. A combination of several characterization techniques, such as polarized optical microscopy (POM), atomic force microscopy (AFM), differential scanning calorimetry (DSC), and X-ray scattering experiments, has been applied to monitor the development of the crystalline structure of the molecular brushes on different length scales ranging from the crystallographic unit cell through single macromolecules to supramolecular spherulites.

Experimental Section

Materials. Linear poly(ε-caprolactone) (M_n = 5000, PDI = 1.49) (LPCL) from Polymer Source, Inc., was used as received. The PCL brush (IA) was synthesized via anionic ring-opening polymerization (AROP) of ε-caprolactone (ε-CL) from a poly(2-hydroxyethyl methacrylate) (PHEMA) macroinitiator (Scheme 1). The ROP process led to formation of linear PCL in addition to the PCL brushes. The fraction of the linear PCL in the PCL-*b*-PBA brushes was reduced below 10% by precipitation into methanol. A small amount of IA was converted into atom transfer radical polymerization (ATRP)[18,19] macroinitiators and subsequently used in the ATRP chain extension of the PCL side chains with PBA, creating the PCL-*b*-PBA block brushes (IIA). The details of the procedures have been discussed in an earlier publication.[12]

The chemical structure of the synthesized molecular brushes depends on the initiation efficiency of both ε-CL from the PHEMA macroinitiator and also the BA from the IA brushlike macroinitiator. The initiation efficiency in the grafting-from process is usually studied by cleaving side chains and comparing their molecular weights with those predicted for quantitative initiation.[20] For PBA side chains, initiation efficiency exceeds 90% at around 10% monomer conversion. Because of much weaker steric congestion in the brushlike macroinitiator and other synthetic conditions that maximize cross-propagation, the efficiency of chain extension from PCL to PBA should significantly exceed 90%. Unlike PBA, one cannot cleave PCL side chains selectively, since the cleavage of the ester group linking PCL with the backbone would be concurrent with PCL chain degradation. Therefore, the nearly quantitative initiation efficiency of the CL grafting from the PHEMA backbone was verified through molecular imaging by AFM. The high uniformity and high initiation efficiency of the ROP step are consistent with successful grafting polylactide side chains from poly(glycidyl methacrylate) backbone.[21] In spite of considerable steric congestion, due to two polylactide chains per one repeating unit of poly(glycidyl methacrylate), the NMR results suggested >90% initiation efficiency for this system. Thus, initiation efficiency for ROP of the PCL side chains in our system should be at least comparable, since there is only one PCL chain per repeating unit of PHEMA.

Materials Characterization. Molecular weight distributions of the PHEMA backbone (I) as well as PCL (IA) and PCL-*b*-PBA (IIA) molecular brushes were determined using a gel permeation chromatograph (GPC) coupled with a multiangle laser light scattering (MALLS) detector from Wyatt Technology (DAWN EOS, 30 mW, λ = 690 nm). In addition to GPC, the weight distributions have been characterized by the AFM-LB technique.[25] Several AFM images with a total number of molecules of about 300 were analyzed to ensure a relative standard deviation of the mean below 3%.

Thermal properties of the synthesized polymers were characterized by differential scanning calorimetry using a DSC 220 from Seiko Instruments, Inc., at a heating and cooling rate of 10 °C/min. All thermal data reported were obtained from the second run. Polarized optical microscopy studies were carried out using a Nikon Microphot-FX microscope equipped with a CCD-IRIS camera (Sony SSC-C374) and Linkam heating stage. The melts were deposited onto a glass microscope slide and heated to T = 100 °C before cooling rapidly and annealing at T = 30 °C from 24 h (LPCL and IA) to 4 days (IIA).

Sample Preparation. Single molecules and thick films of PCL and PCL-*b*-PBA brushes were prepared by spin-casting a dilute chloroform solution (~0.01 wt %) onto freshly cleaved mica. Dense monolayer films were prepared by Langmuir−Blodgett deposition using a KSV-5000 instrument equipped with a Wilhemy plate balance. Milli-Q double-distilled water was used as the subphase (18.2 MΩ·cm). The samples were compressed at 5 mm/min and transferred to mica at a constant pressure of 0.5 mN/m and a room temperature of T = 25 °C. The same procedure was used for the preparation of films of the diblock copolymer encapsulated in linear PBA. For X-ray scattering measurements, oriented fibers of 0.5 mm thickness were prepared by drawing the polymer cooled from the melt to room temperature. It was found that in order to obtain oriented fibers drawing has to be performed at the initial stages of crystallization when the sample contained only nascent

Table 1. Molecular Characterization of PCL-*b*-PBA Brushes by GPC-MALLS and AFM-LB

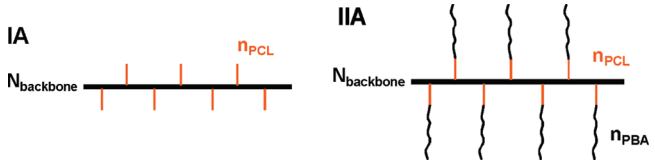

	GPC-MALLS					AFM-LB				
sample	N_{bb}	n_{PCL}[b]	n_{PBA}[c]	M_n	PDI	N_{bb}[a]	n_{PCL}[b]	n_{PBA}[c]	M_n[d]	PDI[e]
IA	450	48	0	2.5×10^6	1.26	449 ± 11	50 ± 3	0	$(2.6 \pm 0.1) \times 10^6$	1.06
IIA-50	450	48	45	5.1×10^6	1.24	451 ± 9	50 ± 3	52 ± 5	$(5.6 \pm 0.6) \times 10^6$	1.04
IIA-150	450	48	182	13×10^6	1.12	448 ± 12	50 ± 3	163 ± 15	$(12 \pm 0.6) \times 10^6$	1.07

[a] From the measured contour length as $N_{bb} = L_n/l_m$, where $l_m = 0.24$ nm is the length of the backbone monomeric unit. [b] $[(M_n(IA)/N_{bb}) - M_{HEMA}]/m_{PCL}$, where $N_{bb} = 450$, $M_{HEMA} = 129$ g/mol, and $m_{PCL} = 114$ g/mol. [c] $[M_n(IIA) - M_n(IA)]/(N_{bb}m_{PBA})$, where $N_{bb} = 450$ and $m_{PBA} = 128$ g/mol. [d] Number-average molecular weight by AFM-LB.[25] [e] Polydispersity index from the contour length measurements PDI $= L_w/L_n \cong M_w/M_n$.

crystallites. Importantly, fibers drawn immediately after quenching from the melt to room temperature do not exhibit any orientation. By contrast, drawing fibers at much more advanced crystallization stages was unsuccessful due to decreased elasticity of the material.

Atomic Force Microscopy. Height and phase micrographs of the films were obtained in tapping-mode using a multimode atomic force microscope (Veeco Metrology group) equipped with Nanoscope IIIA control station and a high-temperature AS-130 VT scanner. Cantilevers with resonance frequencies of about 160 kHz, spring constants of 5.0 N/m, and have tip radii less than 10 nm were used throughout the study. During the in situ heating/cooling of the samples on the heat stage, the cantilever was briefly disengaged, and the resonance tune was checked after temperature equilibration prior to re-engaging. A custom computer software program was used analyze other molecular dimensions such as length and width.

X-ray Scattering. The time- and temperature-resolved small-angle (SAXS) and wide-angle (WAXS) X-ray scattering experiments were performed on the BM26B and ID02 beamlines of the European Synchrotron Radiation Facility (ESRF) in Grenoble (France) using 10 and 12.4 keV X-rays. The SAXS data were collected in transmission using a gas detector. The sample temperature was controlled with a Linkam-DSC heating stage operated under a N_2 flow. The modulus of the scattering vector **s** ($s = 2 \sin \theta/\lambda$, where θ is the Bragg angle and λ the wavelength) was calibrated using several diffraction orders of silver behenate. The WAXS data were collected with a CCD camera. The density of PCL and PBA used for molecular packing calculations are 1.081 g/cm^3 for amorphous PCL,[22] 1.195 g/cm^3 for 100% crystalline PCL,[23] and 1.041 g/cm^3 for PBA.[24]

Results and Discussion

1. Molecular Characterization. Accurate characterization of molecular dimensions of the PCL and PCL-*b*-PBA brush molecules is essential for understanding chain arrangement within both single molecules and bulk samples. For this purpose, every intermediate product was characterized using complementary techniques such as gel permeation chromatography equipped with multiangle laser light scattering (GPC-MALLS) and molecular imaging of Langmuir–Blodgett films by AFM.[25] Both techniques give absolute molecular weight distribution along with number and weight-average molecular weights, i.e., M_n and M_w, respectively. The M_n values were used to calculate the degrees of polymerization for the PCL (n_{PCL}) and PBA (n_{PBA}) blocks. The results are summarized in Table 1. Note that all brushes have the same backbone as evidenced by the AFM measurements of the brush contour length (see N_{bb} columns in Table 1).

The results of the DSC measurements are presented in Figure 1 and summarized in Table 2. Noteworthy is the fact that the linear PCL (LPCL) and brushlike PCL (IA) samples have very similar thermal properties, with nearly identical melting and crystallization temperatures. The glass transition temperatures (T_g) are not obvious for either sample, while the degree of crystallinity (χ_c) of LPCL is slightly higher. In contrast to the homopolymers, both IIA samples show distinctly different thermal behavior. Much lower melting temperatures are observed, which is attributed to smaller PCL crystals. Also observed were two T_g's, one for each block, which indicate microphase separation occurring in the melt. Furthermore, the crystallization peak broadens in IIA-50 and completely vanishes in IIA-150. This is a sign of a slow crystallization process which also results in a lower χ_c. The most significant difference in the crystallization and melting behavior (compared to LPCL and IA) is observed for the IIA-150 sample with the longest PBA block. In section 3, we will provide evidence for PBA-controlled folding of the PCL block, which results in unusually small crystals in IIA-150 samples.

For all four samples, polarized optical microscopy (POM) experiments were conducted to verify the presence of birefringent structures (Figure 2). The most essential difference between the samples concerns their crystallization rate. The crystallization of the LPCL melt at $T = 30$ °C was practically instantaneous, and spherulitic formation was completed within a couple of minutes. For IA, the formation of spherulites was slower than for the LPCL melt, but crystallization was visually complete within 30 min at $T = 30$ °C. Spherulite formation for IIA-50 did not occur as quickly as IA. No nuclei were observed right away, but crystallization became extensive after 30 min and complete by 5 h. As expected, the crystallization of IIA-150 was even slower than that of IIA-50. First, birefringent structures were visualized only after 5 h of annealing at $T = 30$ °C with extensive spherulite formation 4 days after the start of annealing. The observed variations of the crystallization rates are in agreement with the DSC results. The formation of spherulites indicates breakout crystallization of the PCL core block involving neighboring molecular brushes, which occurs despite intramolecular confinement of the PCL block. This behavior is unusual but nonetheless consistent with breakout crystallizationof less constrained linear block copolymers.[26,27]

2. Single Molecule Morphology. The slow crystallization observed by DSC and POM is a result of two microphase separation processes: (i) demixing of the PCL and PBA blocks and (ii) crystallization of the PCL core block. While

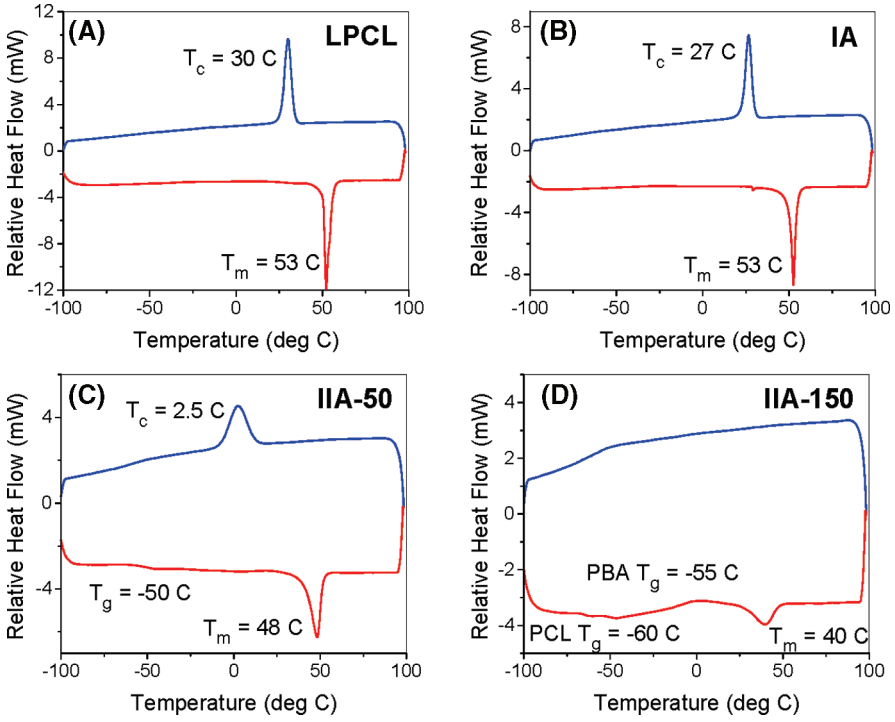

Figure 1. DSC traces for (A) LPCL, (B) IA, (C) IIA-50, and (D) IIA-150 (upper traces = cooling; lower traces = heating). The thermal properties of LPCL and IA are virtually identical, with sharp melting and crystallization temperatures at 53 and 30 °C, respectively. In the case of the IIA-50 sample, lower melting and crystallization transitions are observed. A single glass transition temperature is detected at −50 °C. The IIA-150 sample shows a further depressed melting temperature, while the crystallization peak has completely vanished. In addition, the glass transitions for both PCL and PBA blocks are detected in IIA-150.

Table 2. Summary of DSC Data for Linear PCL, Brushlike PCL (IA), and Block Copolymer Brushes (IIA)

	LPCL	IA	IIA-50	IIA-150
ϕ_{PCL} [a]	1.0	0.98	0.46	0.23
T_m, [b] K	326	326	321	313
ΔH_m, [c] J/g	78 ± 2	73 ± 1	74 ± 1	61 ± 1
ΔS_m, [d] J/(g K)	0.24 ± 0.03	0.22 ± 0.01	0.22 ± 0.03	0.20 ± 0.02
T_c, [e] K	303	300	276	
T_g, [f] K			223 ± 2	213 ± 2 (PCL) 218 ± 2 (PBA)
ΔH_c, [c] J/g	−79 ± 2	−69 ± 1	−74 ± 1	
ΔS_c, [d] J/(g K)	−0.26 ± 0.03	−0.23 ± 0.01	−0.26 ± 0.01	
χ_c [g]	0.58 ± 0.03	0.54 ± 0.03	0.55 ± 0.03	0.45 ± 0.03

[a] Weight fraction of PCL ϕ_{PCL}. [b] Melting temperature. [c] Enthalpy of melting and crystallization of the PCL fraction (ϕ_{PCL}). [d] Entropy of melting and crystallization of the PCL fraction (ϕ_{PCL}). [e] Crystallization temperature. [f] Glass transition temperature. [g] Degree of crystallinity, $\chi_c = \Delta H_m/\Delta H_m°$, where $\Delta H_m° = 135$ J/g is enthalpy of 100% crystalline PCL.[22]

the brushlike architecture favors the core−shell morphology, crystallization of the PCL blocks prefers a lamellar assembly of folded chains. Molecular packing in single molecules (section 2) and in bulk samples (section 3) was carried out.

Figure 3A shows height images of single PCL brush (IA) molecules deposited on a mica substrate. By measuring the number-average contour length (L_n) of the imaged molecules, it was confirmed that the backbone in the adsorbed PCL brushes is fully extended. The length per monomeric unit $l_m = L_n/N_{bb} = 0.22 \pm 0.02$ nm (Table 3) is nearly equal to the length of the monomeric unit $l_0 = 0.24$ nm of the all-carbon backbone in the tetrahedral configuration. In this regard, the PCL molecules behave similar to amorphous brushes,[28] where steric repulsion between the adsorbed side chains causes extension of the backbone.[29,30] The backbone extension weakly depends on the side chain length; however, it exhibits a strong dependence on the grafting density.[31]

Upon "adding" the PBA blocks, however, a remarkable morphological transformation was observed (Figure 3B). Single molecules of brushes with PCL-*b*-PBA side chains exhibit a characteristic spinelike morphology with regularly spaced ribs aligned perpendicular to the backbone, which is reminiscent of polymer shish-kebabs.[32,33] The ribs are present in both IIA-50 and IIA-150, regardless of the film preparation method (Figure S1, Supporting Information). Further proof of their identity was provided by monitoring the melting and subsequent recrystallization of the PCL bundles (Figure S2, Supporting Information).

In addition to the peculiar morphology, one can see a significant fraction of longer molecules randomly distributed throughout monolayer films of IIA-150. This become more evident when comparing larger scale images of PCL and PCL-*b*-PBA brushes in parts C and D of Figure 3, respectively. The corresponding length distributions show that the IIA-150 molecules have a contour length of $L_n = 140 \pm 6$ nm, which is noticeably longer than the length of the PCL brushes ($L_n = 97 \pm 2$ nm). Given that the homopolymer PCL brush is the precursor for the PCL-*b*-PBA brushes, one should expect that IIA-150 molecules cannot be longer than

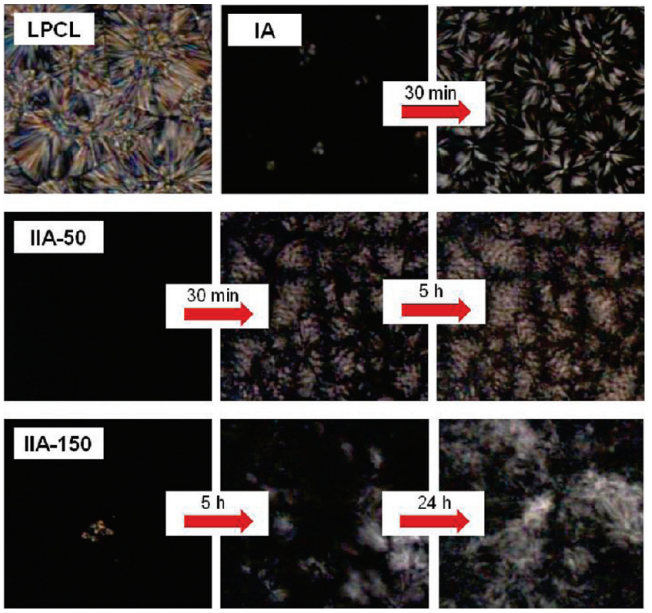

Figure 2. Polarized optical micrographs of LPCL, IA, IIA-50, and IIA-150 samples were obtained after melting at $T = 100$ °C and annealing at $T = 30$ °C. LPCL melt crystallization was rapid, virtually completed within 1 min. The crystallization of the PCL brush (IA) was slower and ended within 30 min at $T = 30$ °C. In contrast, the crystallization of IIA-50 was noticeably slower; i.e., spherulitic nuclei did not appear instantaneously but extensive spherulite formation was observed after 30 min and was complete by 5 h at $T = 30$ °C. For IIA-150, nuclei emerged only after 5 h and slowly grew to a larger spherulite after 24 h and complete crystallization after 4 days at $T = 30$ °C.

the contour length of the backbone $L_n = N_{bb}l_0 = 450 \times 0.24$ nm = 108 nm. Therefore, the formation of longer chains is attributed to the end-to-end association of PCL-*b*-PBA brushes. Figure 4a,b depicts two magnified fragments of IIA-150 images that capture unimers, dimers, trimers, and a ring of the PCL-*b*-PBA brushes designated as 1, 2, 3, and 4, respectively. The images also show two unimer couples (labeled by 1 → 2) just prior to their association into a dimer. The occurrence and subsequent observation of rings is a rare event, with predominant associated structures being linear multimers. Our attempts to perform more quantitative analysis of the multimer distributions have failed due to the broad length distribution of the unimers and seamless junctions of the unimers. In order to hinder the end-to-end association, the PCL-*b*-PBA brushes were embedded into a matrix of linear PBA (10/90 wt/wt). This resulted in a smaller lengths of $L_n = 100 \pm 2$ nm, which became consistent with the contour length of the fully extended backbone. The origin of the molecular association is not clear yet. Presumably, it is driven by crystallization of the PCL core moieties within the PBA matrix. The crystallization also favorably reduces the contact area between the PCL and PBA blocks at the brush end.

Table 3 summarizes all linear dimensions (see Figure 4c) of the IA, IIA-50, and IIA-150 samples that have been measured by AFM. Since IA is the precursor for both IIA brushes, the measured backbone lengths are practically the same and correspond to the fully extended all-trans conformation. The increase in widths from $D = 58$ nm (IA) to $D = 83$ nm (IIA-50) and then $D = 130$ nm (IIA-150) is consistent with the addition of the PBA block. The length of the PCL ribs in the block copolymer brush is larger than the half-width of the homopolymer brushes, which indicates stronger extension of the PCL chains within the block copolymer samples. The corresponding monomer length

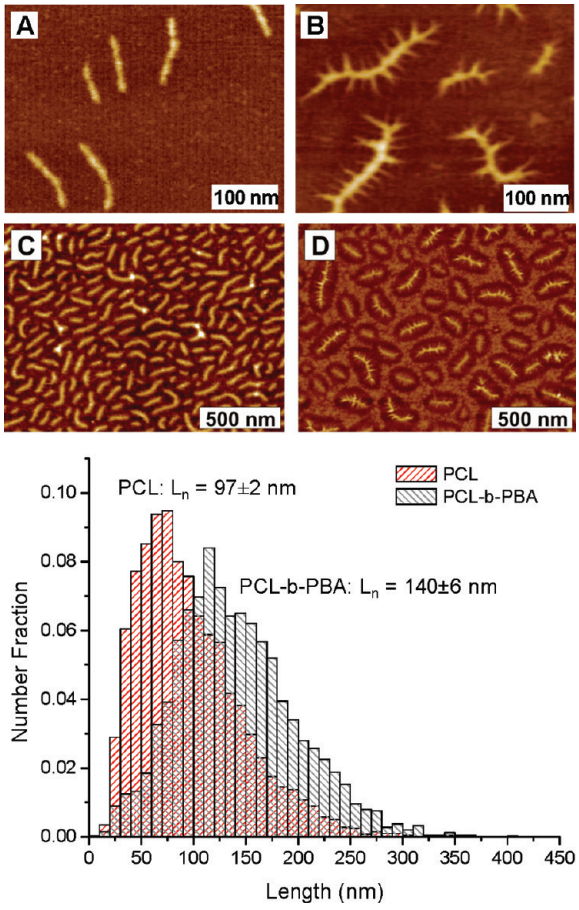

Figure 3. Single brush molecules of (A) IA and (B) IIA-150 spincast on mica. The homopolymer brushes (IA) exhibit the conventional wormlike morphology, while the brushes with block copolymer side chains (IIA-150) reveal a distinctive spinelike morphology with short ribs evenly distributed along the backbone. The larger scale images of (C) IA and (D) IIA-150 samples, prepared by the Langmuir−Blodgett technique, reveal that the block copolymer sample has a significant fraction of longer molecules compared to the homopolymer sample. The corresponding length distributions are consistent with this observation, which is attributed to the end-to-end association of PCL-*b*-PBA brushes.

Table 3. Linear Dimensions of PCL and PCL-*b*-PBA Brushes from Molecular Images by AFM

sample	IA	IIA-50	IIA-150
L_n (nm)[a]	97 ± 2	102 ± 2	100 ± 3
l_m (nm)[b]	0.21 ± 0.01	0.23 ± 0.01	0.22 ± 0.01
D (nm)[c]	58 ± 2	83 ± 1	130 ± 4
L_{PCL} (nm)[d]	29 ± 1	36 ± 2	40 ± 2
L_{PBA} (nm)[e]		13 ± 2	32 ± 6
l_{PCL} (nm)[f]	0.58 ± 0.02	0.72 ± 0.04	0.8 ± 0.04
l_{PBA} (nm)[g]		0.11 ± 0.08	0.15 ± 0.12
d_{PCL} (nm)[h]		14 ± 1	14 ± 1
h_{PCL} (nm)[i]		1.7 ± 1	1.7 ± 1
n[j]		30 ± 3	32 ± 3

[a] Number-average contour length. For IIA, the length was measured for single molecules in a PBA matrix. [b] Length per bb monomer unit = L_n/N_{bb}. [c] Average width of adsorbed brushes. [d] Average width of PCL core (half-width of IA molecules and length of ribs in IIA molecules). [e] Average width of PBA shell = $(D/2) - L_{PCL}$. [f] Length per PCL monomer unit in IA = $D/2n_{PCL}$ and in IIA = L_{PCL}/n_{PCL}. [g] Length per PBA monomer unit = L_{PBA}/n_{PBA}. [h] Distance between the PCL spikes. [i] Thickness of the PCL spikes was measured as $h_{PCL} = h_{PBA} + h_{PCL-PBA} = 0.5$ nm + 1.2 nm, where h_{PBA} is the thickness of the PBA monolayer and $h_{PCL-PBA}$ is the height of the PCL spikes from to the PBA surface from AFM profiles. [j] Number of side chains per rib was calculated for the model in Figure 4C as $m = d_{PCL}/2L_m$, where 2 in the denominator corresponds to two sides of the adsorbed brush.

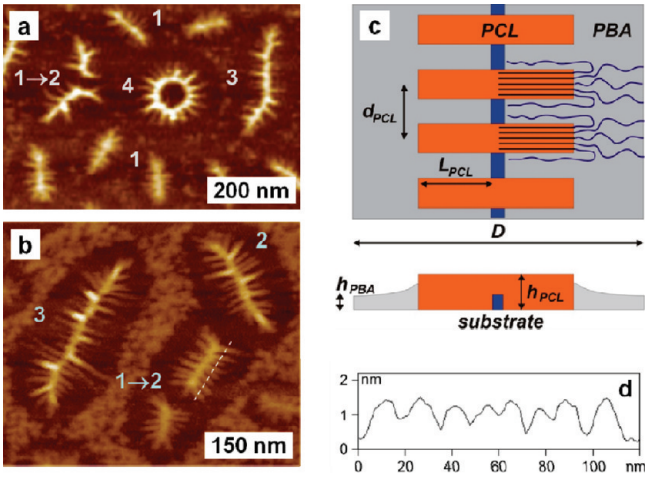

Figure 4. (a, b) AFM height micrographs of IIA-150 single molecules on mica. The numbers 1, 2, 3, and 4 correspond respectively to monomers, dimers, trimers, and cyclic brush molecules that undergo end-to-end association. (c) Model of the spinlike morphology. The adsorbed block copolymer side chains are phase-separated on the substrate to form ribs of fully extended PCL blocks embedded into a matrix of PBA blocks. The latter stabilize the extension of the backbone. (d) Cross-sectional profile along the dashed line in (b) reveals regularly spaced ribs that are assigned to bundles of PCL chains with an average height of $h_{PCL-PBA} = 1.2$ nm (between the top of the ribs and the PBA monolayer) and a spacing of $d_{PCL} = 14 \pm 1$ nm.

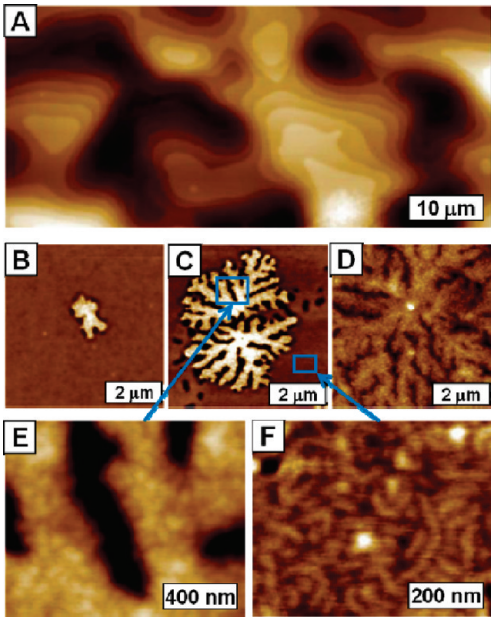

Figure 5. Thick films of IIA-150 brushes. (A) Large-scale height image of terraced films was obtained shortly after spin-casting. (B) On smaller length scales, crystalline nuclei appeared after melting at $T = 100$ °C and annealing at $T = 30$ °C for 1 h and (C) more extensive spherulitic formation after 24 h. (D) Large spherulites appeared after a long annealing time ($T = 30$ °C, $t \sim 1$ month). (E) High resolution of IIA-150 brushes within one of the spherulites reveals grains (see arrow) with a size of 58 nm. (F) Molecular resolution of IIA-150 brushes within a smooth area of the amorphous film indicated by arrow. The brushes visible in the top layer were more cylindrical in shape with shorter backbones and narrower widths than the adsorbed single molecules.

$l_{PCL} = L_{PCL}/n_{PCL}$ ranges from 0.7 to 0.8 nm, which is close to the length $l_0 = 0.86$ nm of the ε-CL monomer. Since the n_{PCL} value was calculated from the brush molecular weight assuming the 100% grafting (Table 1), the close agreement between the brush half-width and the molecular dimensions suggests a nearly 100% grafting efficiency of ε-CL from the PHEMA macroinitiator. Further measurements on IIA-150 show that the regularly spaced ribs ($d_{PCL} = 14 \pm 1$ nm) contain about $m = 32 \pm 2$ side chains each. The area of the rib cross section can be calculated as $S = ma_0 = 32 \times 0.186$ nm$^2 = 5.9$ nm^2, where $a_0 = 0.186$ nm^2 is the area per PCL chain in the (001) plane. From the rib thickness of 1.7 ± 1 nm, one obtains their width of about $5.9/1.7 = 3.5$ nm, which is consistent with cross-sectional profiles measured by AFM along the backbone (Figure 4d).

The ribs are attributed to the interplay of (i) microphase separation between the PCL and PBA blocks, (ii) preferential adsorption of the PBA blocks, and (iii) subsequent crystallization of the PCL blocks into bundles at room temperature. In Figure 4C, we propose a model that rationalizes the chain arrangement within adsorbed macromolecules. The chain packing is dictated by two conditions. First, the maximum area occupied by a brush molecule is limited by the fully extended backbone and side chains (area $< L \times D$); i.e., an individual brush molecule cannot spread beyond a certain footprint. Therefore, there is not enough room to accommodate all side chains on the substrate, which causes partitioning of the side chains into a monolayer of adsorbed chains and a cap of desorbed ones.[31] Second, PBA exhibits stronger adsorption to the underlying substrate (Figure S3, Supporting Information), which increases the area fraction covered by the PBA chains and respectively reduces the substrate coverage by the PCL chains. The preferential adsorption of the PBA blocks under the constraint of the fully extended backbone causes microphase separation of PCL blocks into bundles embedded into a monolayer of PBA blocks. This can be viewed as dewetting of polymer chains that are tethered to an extended backbone. One should emphasize that the extension of the brush backbone is controlled by steric repulsion between the adsorbed PBA chains. This behavior resembles necklacelike structures in polyelectrolyte chains that emerge in poor solvents due to a competition between short-range van der Waals attraction and long-range electrostatic repulsion between charged monomeric units.[34] The bundle formation is additionally favored by crystallization of the PCL blocks within the bundles. Note that despite the weaker adsorption, the PCL chains within the bundles should be fully extended to increase the molecular footprint and thus the number of adsorbed PBA moieties. In other words, no chain folding occurs, as is customary for semicrystalline linear block copolymers crystallized in the bulk or in solution.[35−38]

3. Bulk Samples. Molecular structure of thick films and macroscopic fibers were studied by AFM and X-ray scattering techniques, respectively. AFM studies of the PCL brushes (IA) did not reveal any new features in addition to the optical micrographs in Figure 2. Unlike the homopolymer brushes, however, AFM images of the brushes with block copolymer side chains were more informative. Upon spin-casting, thick films of the IIA-150 sample showed a terraced structure with a step height of about $h = 11 \pm 1$ nm (Figure 5A). After melting at $T = 100$ °C and subsequent annealing at $T = 30$ °C, the samples underwent a very slow transformation from the terraced films to those composed of dendritic morphologies (Figure 5B−D) having a grainy structure (Figure 5E). Similar to linear diblocks,[39,40] the terraces are attributed to microphase-separated layers of core−shell block copolymer brushes. In the flat areas of the largely amorphous films, one achieves molecular resolution showing cylindrical molecules with a width of $D = 37 \pm 2$ nm and length of $L_n = 74 \pm 3$ nm (Figure 5F). The width is larger than the height of the terrace steps and indicates the

flattening of brush molecules at the film surface. Since the cross-sectional area of the imaged molecules ($D \times h = 37 \times 11 = 407 \pm 60$ nm^2) is about the same as the molecular area determined by SAXS $2/\sqrt{3}L_a^2 = 2/\sqrt{3} \times 19^2 = 417$ nm^2, the flattening is attributed to the surface attraction. The measured length corresponds to a length per monomeric unit of $l_m = L_n/N_{bb} = 74/450 = 0.16 \pm 0.01$ nm, which indicates an axial contraction of brushes within thick films relative to the fully extended backbone of adsorbed molecules. In other words, the block copolymer brushes changed their conformation from the spinelike molecules on a substrate (Figure 3B) to cylindrically shaped molecules with a contracted backbone in thick films (Figure 5C). In addition to the flat areas in Figure 5B, one observes small dendritic structures believed to be nuclei of spherulites. After a long annealing time at $T = 30$ °C, these structures has grown into large dendrites surrounded by holes of depleted areas of the film (Figure 5D). These supramolecular structures continued to grow until the film was fully covered with dendrites, as seen after 1 month at $T = 30$ °C (Figure 5E). Close examination of the dendrites revealed grainy structures within the branches that have an average diameter of 58 ± 5 nm (Figure 5F).

A combination of small-angle (SAXS) and wide-angle X-ray scattering (WAXS) techniques has been applied to monitor folding of PCL chains during crystallization, including the variation of crystal thickness, orientation of PCL lamellae, and orientation of PCL chains. Time-resolved SAXS patterns of IA and IIA-150 are presented in Figure 6 while the measured spacing values are summarized in Table 4. In the case of IA, only the peak attributed to the semicrystalline structure of PCL is present at room temperature. This peak vanished upon heating to 70 °C but rapidly reappeared upon cooling to room temperature (Figure 6A). The long period (lamellar domain thickness) for IA is determined to be $L_{SAXS} = 12$ nm, which is significantly shorter than the contour length of the PCL block ($L_{PCL} = 42$ nm for $n_{PCL} = 49$). This implies that the PCL side chains in the fiber are folded upon crystallization. For the IIA-150 fiber, the transformation of the freshly prepared fiber from an initially microphase-separated morphology into a morphology controlled by PCL crystallization was observed (Figure 6B,D). Immediately after quenching, the freshly prepared IIA-150 fiber only had a nonoriented peak (cf. the Sample Preparation section) with a characteristic spacing (domain size) of $L_a = 19$ nm. Since the quenched sample is purely amorphous, this SAXS peak is attributed to microphase separation of the block copolymer side chains. The decrease of intensity and broadening of the copolymer peak occurs upon annealing at room temperature, and then the second peak at $L_{SAXS} = 28$ nm appears after several hours at room temperature. The development of the second peak at the expense of the first one testifies that the crystallization process disrupts the initial block copolymer morphology.

The 2D SAXS patterns recorded on the fibers drawn at the initial crystallization stage at room temperature (Figure 6B) reveal that the crystalline PCL lamellae are oriented parallel to the fiber axis, i.e., the backbone direction. It is likely that the orientation in the fibers is facilitated by the presence of nascent crystallites that act as physical cross-links. Although the crystallization process is not confined to the submolecular scale, the direction of crystal growth is likely to be preferentially selected due to the steric hindrances imposed on the PCL segments by the dense PBA corona. The observed orientation also means that the direction of the PCL chains in the oriented sample is perpendicular to the drawing axis. This follows from the relative positions of the SAXS

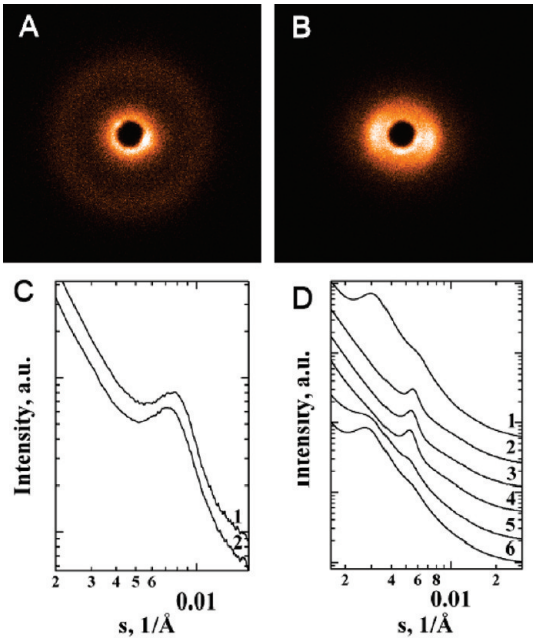

Figure 6. 2D SAXS patterns corresponding to fibers of IA (A) and IIA-150 (B) measured at 25 °C. The fiber axis is vertical. (C) SAXS curves of IA measured at 25 °C on an "old fiber" (1), i.e. the fiber annealed for a long time at 25 °C, and on a "fresh fiber" (2) prepared shortly before the experiment by cooling the sample from 70 to 25 °C. In curves (C1−2), only one peak ($L_{SAXS} = 12$ nm) is observed, which can be assigned to the PCL semicrystalline structure. (D) SAXS curves of IIA-150 measured at 25 °C on an "old fiber" (1), in the melt at 70 °C (2) and upon cooling to 25 °C after different annealing times at 25 °C (0 min, 3; 140 min, 4; 450 min, 5; 1200 min, 6). In the case of IIA-150, the curves reveal the peaks corresponding to the microphase-separated block copolymer structure ($L_a = 19$ nm) and to the semicrystalline structure of the PCL brush ($L_{SAXS} = 28$ nm). The advancing crystallization of PCL brings about an increase in the intensity of the latter peak, which occurs at the expense of the former peak intensity.

Table 4. SAXS Data for the IA, IIA-50, and IIA-150 Polymers

	L_a, nm[a]	$2R_0$, nm[b]	L_{SAXS}, nm[c]	l_{PBA}, nm[d]	l_{PCL}, nm[d]	n_{folds}[e]
IA	11		13		13	3
IIA-50	12	12.4 ± 0.7	22	12.8	9.2	3.5 ± 0.5
IIA-150	19	18.2 ± 1.0	28	22.7	5.3	6.9 ± 1

[a] SAXS distance before crystallization. [b] Calculated as $R_0 = [(M_n/N_A)/(\pi L_n(\phi_{PBA}\rho_{PBA} + \phi_{PCL}\rho_{PCL}))]^{1/2}$ (see section 4). [c] SAXS long period after crystallization. [d] Calculated from eq 1 using $L_{SAXS} = L_{PBA} + L_{PCL}$ (section 4). [e] Calculated from eq 3 (section 4).

peak of the semicrystalline structure and the strong (110) peak of the PCL lattice. The chain orientation has been confirmed by WAXS measurements (Figure 7). The WAXS curves of IIA-150 reveal the characteristic peaks of the orthorhombic unit cell of PCL[41] in the block copolymer brush after annealing at room temperature for a long time (Figure 7A,C). The (110) peak of the orthorhombic unit cell of PCL (Figure 7B) is situated on the meridian (i.e., on the fiber axis direction). Thus, in agreement with the SAXS assignments, the lamellae stacks are parallel to the fiber direction, and the PCL chains in the brush are perpendicular to the fiber direction. The spacing between the (110) reticular planes was measured at $d_{110} = 0.415$ nm, which is very close to the value calculated from the reported lattice parameters.[41] The distance between the crystallographically adjacent positions in the (110) plane, or the projection of the fold length, is $d_{folds} = 0.45$ nm.

4. Molecular Packing: Experiment Interpretation and Comparison with Theory. The molecular dimensions obtained

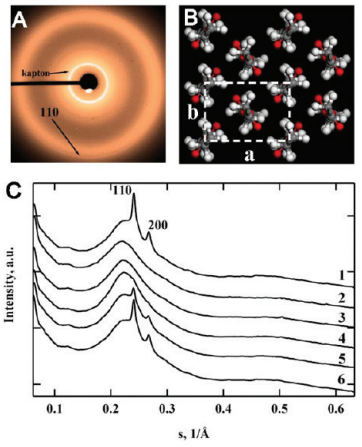

Figure 7. WAXS pattern of a fiber of IIA-150 measured at 25 °C (A). The fiber axis is vertical. The **ab** projection of the orthorhombic unit cell of PCL (B). WAXS curves of IIA-150 corresponding to the same conditions as the ones specified in Figure 6D (C). The appearance of the characteristic peaks of the PCL unit cell is in line with the structure evolution reflected in the SAXS curves (Figure 6D).

Scheme 2. Molecular Packing in Thick Films and Bulk IIA (a) before and (b) after Crystallization of the PCL Core[a]

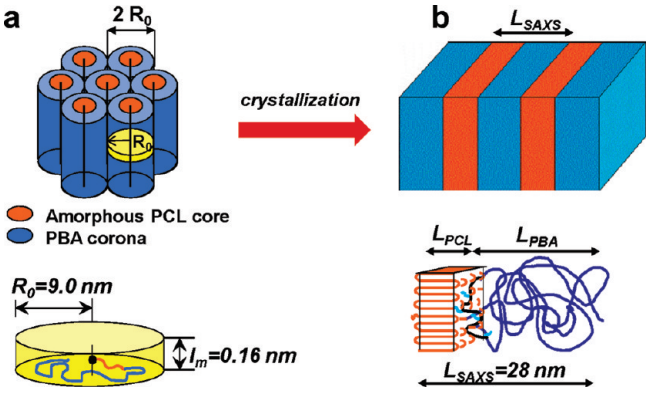

[a] The indicated dimensions (R_0, l_m, and L_{SAXS}) correspond to sample IIA-150. In the amorphous state, the molecules can be modeled as microphase-separated cylinders with a PCL core and PBA shell with a diameter of $2R_0$. Upon crystallization, the initially cylindrical morphology is disrupted by the crystallization of PCL. The block copolymer side chains can be modeled as rectangular lamellae with a thickness L_{SAXS}—the long period from SAXS. The rectangle is composed of two layers: folded chain PCL lamellae and an amorphous layer which includes both the PBA blocks (dark blue) and the PCL disordered segments (light blue). The brush backbone (black) is assumed to segregate at the interface between the two layers to decrease the associated perturbation and thus the energy costs of the crystalline structure.

from SAXS/WAXS can be used to calculate molecular packing models for morphologies prior to and after the PCL crystallization. As shown in Scheme 2a, the molecular packing of the IIA samples before crystallization can be modeled as densely packed cylinders with radius R_0 and length $L_n = 74 \pm 3$ nm, i.e., the number-average length of the molecular brushes in bulk samples (Figure 5F). From the number-average molecular weight (M_n in Table 1) one calculates the radius as

$$R_0 = \sqrt{\frac{V}{\pi L_n}} = \sqrt{\frac{M_n/N_A}{\pi L_n(\phi_{PBA}\rho_{PBA} + \phi_{PCL}\rho_{PCL})}}$$

where N_A is the Avogadro number and $\rho_{PCL} = 1.081$ g/cm^3 and $\rho_{PBA} = 1.041$ g/cm^3 are mass densities for amorphous PCL[23] and amorphous PBA,[24] respectively. As shown in Table 4, the calculated diameter $D = 2R_0$ values are in good agreement with the corresponding L_a distances measured by SAXS.

Crystallization of the PCL block is evidenced by the development of the second peak at $L_{SAXS} = 28$ nm (Figure 6D). As shown in Scheme 2b, this spacing is attributed to the long period of alternating crystalline and amorphous layers and can be written as $L_{SAXS} = L_{PBA} + L_{PCL}$. The ratio of the PBA and PCL layer thickness can be estimated by

$$\frac{l_{PBA}}{l_{PCL}} = \frac{M_{PBA}}{M_{PCL}}\frac{\rho^C_{PCL}}{\rho_{PBA}} = \frac{n_{PBA}}{n_{PCL}}\frac{m_{BA}}{m_{CL}}\frac{\rho^C_{PCL}}{\rho_{PBA}} \cong 1.3\frac{n_{PBA}}{n_{PCL}} \quad (1)$$

where $m_{BA} = 128$ g/mol and $m_{CL} = 114$ g/mol are molar masses of the BA and CL monomeric units, respectively; $\rho^C_{PCL} = 1.194$ g/cm is mass density of crystalline PCL.[23] Equation 1 has been used to calculate the PCL thickness $L_{PCL} = 5.3$ nm. This is less than the PCL lamella thickness $L = 8$ nm measured for linear PCL chains[42] and suggests that the amorphous PBA block controls folding of the PCL block. In this calculation, the degree of crystallinity of the PCL blocks is assumed to be 100%. For lower crystallinity, one would obtain an even smaller value for the thickness of the PCL crystals. As shown in Scheme 2B, the crystallinity of PCL in the brush has to be reduced as compared to linear chains due to steric hindrances imposed by the branching points. The PCL sequences close to the backbone cannot be easily accommodated in the PCL lamellae because of the incommensurability of the distance between the branching points and d_{folds}. As for the PBA chains, given that $L_{PBA} = 22.7$ nm, the chains are thought to be coiled and interdigitated with neighboring PBA blocks.

From the length of the crystalline PCL domain (L_{PCL}) one can calculate the number of folds as

$$n_{folds} = \frac{L_0}{L_{PCL}} - 1 \quad (2)$$

where $L_0 = n_{PCL}l_{CL}$ nm is the contour length of the PCL block and $l_{CL} = 0.86$ nm is the length of the CL monomeric unit. By combining eqs 1 and 2, one obtains the following equation for the number of folds as a function of the amorphous block only:

$$n_{folds} = 1.1\frac{n_{PBA}}{n_{PBA}} - 1 \quad (3)$$

Table 4 summarizes the SAXS data including the thickness of amorphous PBA and crystalline PCL domains (L_{PBA} and L_{PCL}) and the number of folds per PCL block. It can be seen that by increasing the length of the PBA block one makes the crystals even thinner, as compared to those formed by pure PCL brush or by linear PCL chains.[43]

The ability to control the thickness of polymer crystallites in the block copolymer brushes is in contrast to the homopolymer crystalline polymer case where chain folding is a kinetic effect. To predict the equilibrium size of the crystalline domain, DiMarzio et al.[38] and Birstein and Zhulina[36] considered lamella of linear block copolymers as a folded-chain lamellae sandwiched between amorphous domains. The main contributions into the total free energy are the elasticity of the amorphous chains and the interfacial energy. By minimizing the total free energy with respect to the area

Table 5. Melting Points Determined by DSC and Calculated from Gibbs−Thomson Equation

	T_m, K (DSC)	L_{PCL}, nm (SAXS)	T_m^{calc}, K[b]
LPCL	326	12[a]	337
IA	326	13	338
IIA-50	321	9.2	330
IIA-150	313	5.3	308

[a] Linear PCL thickness from Gedde et.al.[44] [b] Calculated from eq 5.

per chain, they have obtained the following expression for the size of the thickness of the crystalline domain:

$$L_c = n_c n_a^{-1/3} \quad (4)$$

In our paper, L_c, n_c, and n_a correspond to L_{PCL}, n_{PCL}, and n_{PBA}, respectively. From Table 4, one obtains $L_{PCL}^{IIA\text{-}150}/L_{PCL}^{IIA\text{-}50} = 0.6 \pm 0.2$ and $(n_{PBA}^{IIA\text{-}150}/n_{PBA}^{IIA\text{-}50})^{-1/3} = 0.7 \pm 0.2$, which are in reasonable agreement with eq 4.

The size of the crystalline domains also affects the melting temperature, which can be calculated using the Gibbs−Thomson equation

$$T = T_m^{\infty}\left[1 - \frac{2\sigma_e}{L_{PCL}\Delta H_m^{\circ}\rho_{PCL}^{C}}\right] \quad (5)$$

where $T_m^{\infty} = 359$ K is melting point of an infinite size PCL crystal,[44] $\sigma_e = 60$ mJ/m^2 is the fold surface energy,[45] L_{PCL} is crystal thickness determined from SAXS, $\Delta H_m^{\circ} = 135$ J/g is the enthalpy of fusion of 100% PCL,[22] and $\rho_{PCL}^{C} = 1.19$ g/cm^3 is the density of crystalline PCL.[23] The calculated values for LPCL, IA, IIA-50, and IIA-150 molecules are summarized in Table 5 along with the experimentally determined T_m values from DSC. The melting transitions for LPCL and IA are similar due to the similar size of the crystalline domains. For the block copolymer brushes, both calculated and experimentally determined T_m values follow a decreasing trend with decreasing mass fraction of PCL as expected. The observed discrepancy between the calculated and measured temperature values are ascribed to unknown variations of the crystal surface energy due to adhesion and elasticity of the PBA block. Note that T_m is very sensitive to small variations in σ_e; e.g., 3% increase in σ_e would cause ca. 10 K decrease of the melting temperature.

Conclusion

The structure formation in the densely grafted brushes with PCL-*b*-PBA diblock copolymer side chains experiences a complex interplay between microphase separation of the chemically different blocks and crystallization of the core block. This results in the unusual morphologies and provides an opportunity to control the crystallization process both in thin films and in the bulk by changing the block ratio and grafting density. Upon adsorption, the molecules adopt a spinelike morphology of crystalline spines of PCL surrounded by the amorphous corona of PBA. This morphology is caused by preferential adsorption of the PBA corona to the substrate and subsequent crystallization of the PCL core. In bulk samples, molecular brushes are initially segregated adopting a shape of amorphous cylinders with the PCL core surrounded by the PBA corona. The crystallization process disrupts the molecularly segregated morphology and results in a layered crystalline/amorphous structure with a very different periodicity. Optical observation of nascent spherulitic morphology testifies that crystallization proceeds by breaking out the core−shell structure of individual molecules to form a supramolecular assembly of PCL lamellae on much larger length scales. Although the crystallization process is not confined to the submolecular scale, the direction of crystal growth in oriented fibers is preferentially selected likely due to the steric hindrances imposed on the PCL segments by the dense PBA corona. Effectively, molecular brushes with block copolymer side chains serve as templates for crystallization of the core block while the template structure is stabilized by the amorphous polymer corona. This allowed for the alignment of the PCL lamellae during crystallization of extruded fibers. In addition, the amorphous corona block controls folding of the PCL chains and thus the thickness of the crystalline domains.

Thus, the crystallization of the studied macromolecules is very different from both linear block copolymers and main-chain columnar liquid crystals. Unlike linear diblocks, the breakout crystallization of the core−shell molecular brushes is a much slower process, which, under certain conditions, can preserve molecular alignment within extruded fibers. Unlike the main-chain liquid crystals, where the crystallization of the extended polymer backbones requires only a little rearrangement,[46−48] the formation of the crystalline phase in molecular brushes involves a complete reconfiguration of the side chains. This makes the epitaxial mechanism of crystal growth within the parent columnar mesophase impossible. The observed mechanism of the crystallization templating can prove useful in designing complex nanostructured materials.

Acknowledgment. We gratefully acknowledge funding from the National Science Foundation (DMR 0606086, CBET-0609087) and Petroleum Research Fund (46204-AC7). We also acknowledge the European Synchrotron Facility for provision of synchrotron radiation facilities. We thank W. Bras, T. Narayanan, and M. Sztucki for assistance in synchrotron experiments. We are grateful to E. B. Zhulina and M. Rubinstein for very helpful and stimulating discussions.

Supporting Information Available: Single brush molecules of IA, IIA-150, and IIA-50 on mica (Figure S1); AFM heating and cooling of single molecules of IIA-150 brushes (Figure S2); film pressure−molecular area isotherms on a water substrate measured for PBA and PCL brushes along with two brushes with PCL-*b*-PBA block-copolymer side chains IIA-50 and IIA-150 (Figure S3). This material is available free of charge via the Internet at http://pubs.acs.org.

References and Notes

(1) Ivanov, D. A.; Amalou, Z.; Magonov, S. N. *Macromolecules* **2001**, *34*, 8944–8952.
(2) Ivanov, D. A.; Bar, G.; Dosière, M.; Koch, M. H. J. *Macromolecules* **2008**, *41*, 9224–9233.
(3) Shin, K.; Woo, E.; Jeong, Y. G.; Kim, C.; Huh, J.; Kim, K. *Macromolecules* **2007**, *40*, 6617–6623.
(4) Woo, E.; Huh, J.; Jeong, Y. G.; Shin, K. *Phys. Rev. Lett.* **2007**, *98*, 136103.
(5) Xiang, H.; Shin, K.; Kim, T.; Moon, S. I.; McCarthy, T. J.; Russell, T. P. *Macromolecules* **2004**, *37*, 5660–5664.
(6) Kageyama, K.; Tamazawa, J.; Aida, T. *Science* **1999**, *285*, 2113–2115.
(7) Leibler, L. *Macromolecules* **1980**, *13*, 1602–1617.
(8) Thurn-Albrecht, T.; Schotter, J.; Kastle, G. A.; Emley, N.; Shibauchi, T.; Krusin-Elbaum, L.; Guarini, K.; Black, C. T.; Tuominen, M. T.; Russell, T. P. *Science* **2000**, *290*, 2126–2129.
(9) Zhu, L.; Cheng, S. Z. D.; Calhoun, B. H.; Ge, Q.; Quirk, R. P.; Thomas, E. L.; Hsiao, B. S.; Yeh, F.; Lotz, B. *Polymer* **2001**, *42*, 5829–5839.
(10) Zhu, L.; Cheng, S. Z. D.; Calhoun, B. H.; Ge, Q.; Quirk, R. P.; Thomas, E. L.; Hsiao, B. S.; Yeh, F.; Lotz, B. *J. Am. Chem. Soc.* **2000**, *122*, 5957–5967.
(11) Loo, Y.; Register, R. A.; Ryan, A. J. *Macromolecules* **2002**, *35*, 2365–2374.

(12) Lee, H.-i.; Jakubowski, W.; Matyjaszewski, K.; Yu, S.; Sheiko, S. S. *Macromolecules* **2006**, *39*, 4983–4989.
(13) Sheiko, S. S.; Möller, M. *Chem. Rev.* **2001**, *101*, 4099–4123.
(14) Zhang, M.; Müller, A. H. E. *J. Polym. Sci., Part A: Polym. Chem* **2005**, *43*, 3461–3481.
(15) Zhang, B.; Grohn, F.; Pedersen, J. S.; Fischer, K.; Schmidt, M. *Macromolecules* **2006**, *39*, 8440–8450.
(16) Rathgeber, S.; Pakula, T.; Wilk, A.; Matyjaszewski, K.; Lee, H-I.; Beers, K L. *Polymer* **2006**, *47*, 7318–7327.
(17) Sheiko, S. S.; Sumerlin, B. S.; Matyjaszewski, K. *Prog. Polym. Sci.* **2008**, *33*, 759–785.
(18) Matyjaszewski, K.; Xia, J. *Chem. Rev.* **2001**, *101*, 2921–2990.
(19) Matyjaszewski, K.; Tsarevsky, N. V. *Nat. Chem.* **2009**, *1*, 276–288.
(20) Neugebauer, D.; Sumerlin, B. S.; Matyjaszewski, K.; Goodhart, B.; Sheiko, S. S. *Polymer* **2004**, *45*, 8173–8179.
(21) Huang, K.; Rzayev, J. *J. Am. Chem. Soc.* **2009**, *131*, 6880–6885.
(22) Crescenzi, V.; Manzini, G.; Calzolari, G.; Borri, C. *Eur. Polym. J.* **1972**, *8*, 449–463.
(23) Chatani, Y.; Okita, Y.; Hiroyuki, T.; Yamashita, Y. *Polym. J.* **1970**, *1*, 555–562.
(24) Barlow, A. J.; Day, M.; Harrison, G.; Lamb, J.; Subramanian, S. *Proc. R. Soc. London A* **1969**, *309*, 497–520.
(25) Sheiko, S. S.; da Silva, M.; Shirvaniants, D.; LaRue, I.; Prokhorova, S.; Moeller, M.; Beers, K.; Matyjaszewski, K. *J. Am. Chem. Soc.* **2003**, *125*, 6725–6728.
(26) Kim, G.; Han, C. C.; Libera, M.; Jackson, C. L. *Macromolecules* **2001**, *34*, 7336–7342.
(27) Balsamo, V.; Gyldenfeldt, F. v.; Stadler, R. *Macromol. Chem. Phys.* **1996**, *197*, 3317–3341.
(28) Sheiko, S. S.; Prokhorova, S. A.; Beers, K. L.; Matyjaszewski, K.; Potemkin, I. I.; Khokhlov, A. R.; Moeller, M. *Macromolecules* **2001**, *34*, 8354–8360.
(29) Sheiko, S. S.; Sun, F. C.; Randall, A.; Shirvanyants, D.; Rubinstein, M.; Lee, H.; Matyjaszewski, K. *Nature* **2006**, *440*, 191–194.
(30) Panyukov, S.; Zhulina, E. B.; Sheiko, S. S.; Randall, G. C.; Brock, J.; Rubinstein, M. *J. Phys. Chem. B* **2009**, *113*, 3750–3768.
(31) Lord, S. J.; Sheiko, S. S.; LaRue, I.; Qin, S.; Lee, H.-I.; Matyjaszewski, K. *Macromolecules* **2004**, *37*, 4235–4240.
(32) Pennings, A. J.; Kiel, A. M. *Kolloid Z. Z. Polym.* **1965**, *205*, 160–165.
(33) Kimata, S.; Sakurai, T.; Nozue, Y.; Kasahara, T.; Yamaguchi, N.; Karino, T.; Shibayama, M.; Kornfield, J. A. *Science* **2007**, *316*, 1014–1017.
(34) Dobrynin, A. V.; Rubinstein, M.; Obukhov, S. P. *Macromolecules* **1996**, *29*, 2974–2979.
(35) Hamley, I. W. *Adv. Polym. Sci.* **1999**, *148*, 113–137.
(36) Birshtein, T. M.; Zhulina, E. B. *Polymer* **1990**, *31*, 1312–1320.
(37) Whitmore, M. D.; Noolandi, J. *Macromolecules* **1988**, *21*, 1482–1496.
(38) DiMarzio, E. A.; Guttman, C. M.; Hoffman, J. D. *Macromolecules* **1980**, *13*, 1194–1198.
(39) Liang, G.; Xu, J.; Fan, Z.; Mai, S.; Ryan, A. J. *Polymer* **2007**, *48*, 7201–7210.
(40) Liang, G.; Xu, J.; Fan, Z.; Mai, S.; Ryan, A. J. *J. Phys. Chem. B* **2006**, *110*, 24384–24389.
(41) Tadokoro, H. In *Structure of Crystalline Polymers*; Krieger Publishing Co.: Malabar, FL, 1990.
(42) Li, B.; Wu, Y.; Liu, M.; Esker, A. R. *Langmuir* **2006**, *22*, 4902–4905.
(43) Basire, C.; Ivanov, D. A. *Phys. Rev. Lett.* **2000**, *85*, 5587.
(44) Núñez, E.; Ferrando, C.; Malmström, E.; Claesson, H.; Werner, P.; Gedde, U. W. *Polymer* **2004**, *45*, 5251–5263.
(45) Heck, B.; Hugel, T.; Iijima, M.; Sadiku, E.; Strobl, G. *New J. Phys.* **1999**, *1*, 17.
(46) Gearba, R. I.; Anokhin, D. V.; Bondar, A. I.; Godovsky, Y. K.; Papkov, V. S.; Makarova, N. N.; Magonov, S. N.; Bras, W.; Koch, M. H. J.; Masin, F.; Goderis, B.; Ivanov, D. A. *Macromolecules* **2006**, *39*, 988–999.
(47) Gearba, R. I.; Dubreuil, N.; Anokhin, D. V.; Godovsky, Y. K.; Ruan, J.; Thierry, A.; Lotz, B.; Ivanov, D. A. *Macromolecules* **2006**, *39*, 978–987.
(48) Defaux, M.; Vidal, L.; Möller, M.; Gearba, R. I.; DiMasi, E.; Ivanov, D. A. *Macromolecules* **2009**, *42*, 3500–3509.